

Gold Nanoparticles Effect on (Bi,Pb)-2223 Superconducting Thin Films

Saad F. Oboudi¹ & Mustafa Q. AL-Habeeb¹

¹ Department of Physics, College of Science, University of Baghdad, Al-Jadriya, Baghdad, Iraq

Correspondence: Saad F. Oboudi, Department of Physics, College of Science, University of Baghdad, Al-Jadriya, Baghdad, Iraq. E-mail: saadoboudi@gmail.com

Received: September 5, 2016 Accepted: September 14, 2016 Online Published: September 30, 2016

doi:10.5539/apr.v8n5p64

URL: <http://dx.doi.org/10.5539/apr.v8n5p64>

Abstract

Superconductor samples were prepared by a conventional solid-state reaction method and systematically studied for their superconducting properties. The Au nanoparticles concentration x varied from 0.0 to 1.0 wt% of the sample's total mass. Those samples were used as targets to prepare $\text{Au}_x\text{-Bi}_{1.7}\text{Pb}_{0.3}\text{Sr}_2\text{Ca}_2\text{Cu}_3\text{O}_{10+\delta}$ thin films by pulsed laser deposition (PLD), deposited on Si (111) substrates and post-deposition oxygen annealing have been achieved. The effect of Au nanoparticles (20 nm) on the physical properties of superconducting phase was studied. The phase identification/gross structural characteristics of synthesized bulk and thin films samples explored through powder X-ray diffractometer and reveals that all the samples crystallize in orthorhombic structure. In addition, phase examination by XRD indicated that Au nanoparticles enhanced the (Bi,Pb)-2223 phase formation. The critical transition temperature (T_c) measured by the standard DC four-probe method and was found to have optimal value at $x=1.0$ wt%, which had a maximum enhancement in T_c for both bulk and thin films samples. The surface morphology investigated through scanning electron microscope (SEM) and atomic force microscopy (AFM), the granular investigation showed that both number and size of voids decreased while grains size increased as x increases to 1.0 wt%.

Keyword: Bi(Pb)-2223, Au nanoparticle, solid state reaction, Pulsed Laser Deposition.

1. Introduction

Since the discovery of the bismuth-based superconductors (Maeda, Tanaka, Fukutomi, & Asano, 1988), varieties of potential applications of bulk material (Verma et al., 2012; Díaz-Valdés et al., 1993) as well as thin films (Mua, Sundaresan, kman, & Dung, 2014; Jannah, Halim, & H. Abdullah, 2009) have been reported. The interest is mainly due to the great potential of this material for use in superconductor devices. It has been found that the nominal composition and thermal treatment parameters such as annealing temperature, annealing time, and heating and cooling rates play an important role in the formation of high- T_c phases (Abbas, Oboudi, & Raof, 2015). Different doping and substitution materials have been used to improve formation and stability of the Bi-2223 phase. Pb is the most important doping element that influences the microstructure, phase composition, and the related superconducting properties of the BSCCO system. The presence of Pb in the initial mixture favors the reaction kinetics of the 110 K (Bi-2223) phase by partial substitution of bismuth (Bi) (Jeremie, Alami-Yadri, Grivel, & Flükiger, 1993). However, it is difficult to obtain pure high T_c phase Bi-2223 during synthesis, but it is still one of the important materials that have been investigated extensively (Sozeri, Ghazanfari, Ozkan, & Kilic, 2007).

The presence of inter-grain voids, impurity phases, oxygen vacancies, inhomogeneous microdefects, etc., in its bulk form due to granular nature affects the performance of the superconductor compound. This issue can, however, be resolved up to some extent by filling the pores with some suitable nanostructures at inter-granular sites in the bulk superconductor. The effects of nanostructures addition on the physical and structural properties of different high temperature superconducting families in their bulk as well as thin films were studied by different research groups to improve the superconducting properties (Jabbar, Qasim, Mumtaz, & Nadeem, 2015; Zelati, Amirabadizadeh, Kompany, & Salamati, 2014; Hafiz & Abd-Shukor, 2015). Generally, it is observed from the literatures that the addition of nanostructures in HTSCs improves the inter-grain connectivity and superconductivity parameters up to certain extent without affecting their crystal structures, also enhances the additional pinning effects in the bulk polycrystalline samples for the improvement of in-field superconducting

properties (Farbod & Batvandi, 2011; Miura et al., 2006; Mumtaz, Khan, & Khan, 2010; Nadeem et al., 2014). Recently, the effect of nano addition has been extensively studied to improve the superconducting properties such as nano elements: (Ag, Au, etc) (Suazlina et al., 2014), nano oxide's (SnO₂, ZrO₂, MgO, etc) (Ishii & Hatano, 2000) and nano compound: (NiFe₂O₄, BiFeO₃, etc) (Suvasis, 2011).

Several physical and chemical techniques (Ki Young & Soo Lee, 2006; Hermiz, Abbass, & Gilioli, 2009; Ramadan, Abdel-Hady, Abdel-Ghany, & Soltan, 2000), such as pulsed laser deposition (PLD), molecular beam epitaxy, R. F. sputtering, co-evaporation, spray pyrolysis technique and chemical vapour deposition (CVD) have been used to prepare superconducting thin films. The PLD method is known to be suitable for fabricating films with complex stoichiometry and become a potential method in fabricating highly quality superconducting thin films suitable for electronic applications such as in Josephson junction based electronics and in second generation coated conductors. Significant efforts have been done by researchers to improve the critical temperature for textured and epitaxial HTSc thin films and its potential applications. Whereas the investigation of nano particles influence on superconductors is very important from the viewpoint of practical application. In this work, Au nano-particles was added to Bi(Pb)-2223 superconductor system, the structure, phase formation and electrical properties were investigated. Thin films of Bi(Pb)-Sr-Ca-Cu-O with and without Au nanoparticles addition were post annealed. The influence of optimal processing parameters on the formation of the superconducting thin films was investigated.

2. Materials and Methods

Samples of Bi_{1.7}Pb_{0.3}Sr₂Ca₂Cu₃O_{10+δ} with different addition concentration of Au nanoparticles were prepared by a conventional solid state reaction method. The stoichiometric amounts of high purity powders of Bi₂O₃, Pb₃O₄, Sr(NO₃)₂, CaO and CuO were used as starting materials. Au nanoparticles were added by weight percentages (0.0, 0.2, 0.4, 0.6, 0.8 and 1.0 weight %). The powders were mixed together by using of mill machine (SPEX Industries Inc.-USA), for a period of 10 minute, The mixture homogenization takes place by adding a sufficient quantity of 2-propanol to form a paste during the process of grinding for about 30 minutes. The mixture was grounded to a fine powder and then calcined by using a tube furnace at 810°C for 24 h. The mixture then pressed into pellets of diameter 13 mm and thickness (2-3) mm by using hydraulic press type (SPECAC) under a pressure of 0.7 GPa. The pellets were sintered in air at 845°C for 140 hr with a heating and cooling rate of 2°C/min. These pellets were used as targets to prepare superconductor thin films by using pulsed laser deposition technique. The targets were entered in vacuum chamber 10⁻² mbar, and Q-switched Nd:YAG pulse laser operated at 1064 nm wavelength, 500 mJ/pulse, the distance between substrate and target 2 cm and 700 mJ pulse energy for frequency 5 Hz. All samples were grown at an optimal p-type Si (111) substrate at room temperature. The as-deposited thin films were post annealed in a tube furnace under 2 lit/min of oxygen flow at 800°C for 1.5 h with heating and cooling rate of 5°C/min. Resistance-temperature data were obtained by using four point probe DC method at temperature range (77 - 300) K to determine the critical temperature (*T_c*). All samples were subjected to gross structural characterization by X-ray diffraction (XRD) (Shimadzu-6000, with Cu-Kα source). A computer program was used to calculate the lattice parameters, based on Cohen's least square method. The surface morphology of the samples was carried out by scanning electron microscopy (SEM) performed by (FEI Co. system SN: 9922650 – 2013/ Holland) and atomic force microscopy (AFM) type origin USA Model (AA300-CSPM).

3. Results and Discussion

X-ray diffraction pattern of samples with Au nanoparticles addition (*x*= 0.0, 0.2, 0.4, 0.6, 0.8 and 1.0) are shown in Figure 1. It is more suitable for pointing out the presence of both phases Bi(Pb)-2223 and Bi(Pb)-2212 with Bi(Pb)-2223 being the dominant one, in addition to weak impurity phases of Ca₂PbO₄ peak at $2\theta = 17.4^\circ$ and Sr₂Ca₂Cu₇O peak at $2\theta = 36.8^\circ$ in some nano-Au added samples. The appearance of more than two phases could be related to the stacking faults along the *c*-axis. To estimate the volume fraction of the phases, we used the corresponding Bi-2212 and Bi-2223 peaks, as in the following formulas (Zargar Shoushtari & Mousavi Ghahfarokhi, 2011):

$$V_{H(Bi-2223)} = \frac{\sum I(2223)}{\sum I(2223) + \sum I(2212) + \sum I_{other}} \times 100\% \quad (1)$$

$$V_{L(Bi-2212)} = \frac{\sum I(2212)}{\sum I(2223) + \sum I(2212) + \sum I_{other}} \times 100\% \quad (2)$$

It can be seen that the intensity of several peaks such as (002) at $2\theta = 6.5^\circ \mp 0.5^\circ$ to (1023) at $2\theta = 59.8^\circ \mp 0.5^\circ$ for Bi-2223 phase has been increased with the increasing of Au addition concentration. Also, the

peaks positions for these samples are shifted towards higher 2θ values. This could be attributed to the replace between the atomic sites within Bi-2223 cuprates and representing the influence of Au nanoparticles on crystallization of the grains. This observation is also associated with broadening of some peaks due to the spacing between the peaks or overlapping of 2223-phase with 2212-phase as in (0.8 and 1.0)wt.% samples. Similar behavior were obtained by Mawassi et al. (2014), Ahmad (2015) for different compounds. The XRD patterns indicate that all the samples are well-crystallized orthorhombic. The impurity phases Ca_2PbO_4 and $\text{Sr}_2\text{Ca}_2\text{Cu}_7\text{O}$ have an effect on the volume fraction and the lattice parameters especially the c-axis. The lattice parameters a , b , c and c/a unit cell volumes and the volume fractions of the phases for Au nanoparticles added samples are listed in Table 1.

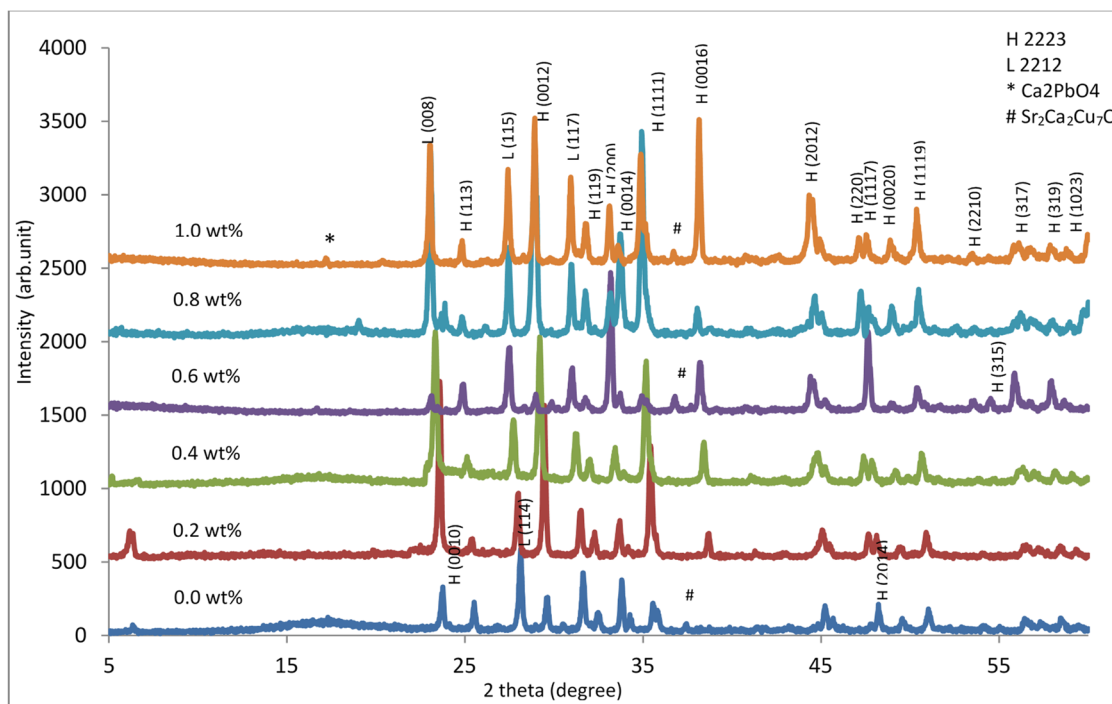


Figure 1. X-Ray diffraction patterns of Bi(Pb)-2223 for different Au nanoparticles added samples

Table 1. Lattice parameters and unit cell volumes of (Bi,Pb)-2223 samples with different Au nanoparticles addition

(Au NPs)wt%	a Å	b Å	c Å	V (Å) ³	$\frac{c}{a}$	ρ_M (g/cm ³)	Volume Fraction	
							HT _c %	LT _c %
0.0	5.412432	5.429031	37.06188	1089.0359	6.849	1.561	58.61	41.39
0.2	5.433565	5.453164	37.05394	1097.9127	6.819	1.548	58.71	41.29
0.4	5.450231	5.460859	37.06619	1103.1991	6.801	1.541	60.26	39.74
0.6	5.458755	5.524594	37.01653	1116.3224	6.781	1.522	60.77	39.23
0.8	5.458275	5.497732	37.21566	1116.7724	6.818	1.522	71.77	28.23
1.0	5.451291	5.526623	37.29641	1123.6375	6.842	1.513	77.24	22.76

The DC electrical resistance reveals the resistivity of the samples as shown in Figure 2. All the samples exhibit metallic behavior in the variation of resistivity versus temperature measurements at high temperatures before superconducting transition. It is interesting to note that all the gold nanoparticle added samples show higher T_c values than 0.0 wt% nano-Au sample. Addition of nano-Au shows a highest T_c at the maximum Au nanoparticles addition concentration $x=1.0$ wt%. This is compatible with Lee (2003) and Ozturk et al. (2007). Increasing the T_c value is probably due to the improvement of weak links between the superconducting grains through the healing of a higher voids and pores with increasing Au nanoparticles. In this case Au-nano added

samples show along with T_c and $T_{c R=0}$ values, which predicts the optimal insertion level of nanoparticles (Au)_x/Bi(Pb)-2223 matrix (Soo Lee, 2003). Superconducting fluctuations in the superconducting transition contribute to the critical temperature (T_c) and these particular Au nanoparticles addition may enhance these fluctuations and can influence T_c of these compounds and causes the suppression of superconductivity parameters.

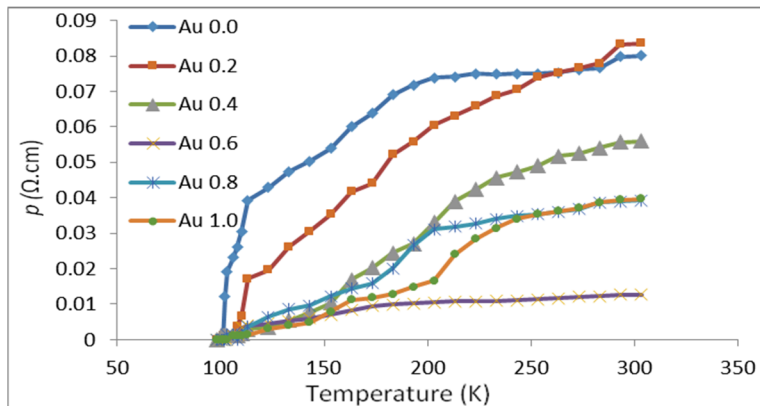


Figure 2. ρ -T plots for different Au nanoparticles added samples

Furthermore, the superconducting volume fraction can also be improved by optimizing oxygen, which can occupy oxygen vacancies in the samples. This applies to the addition of Au nanoparticles, but Au-nano is most influential for improving weak links at the grain boundaries, i.e. the improvement or destruction has occurred in the inter-grain connectivity, as referred to by Jabbar et al. (2015). It can be observed that the δ values for the samples, as in Table (2) are in a range between (0.0437 and 0.394), these values are convincing. But the oxygen atoms in the basal plane of the unit cell tend to align in series along one of the crystal axes (by agreement taken as the b -axis) when the oxygen content (x) exceeds ≈ 0.35 . The chain formation is accompanied by the structural transition from a tetragonal state to a weakly distorted orthorhombic state, as in nano-Au (0.6 wt%) sample, which has the a value (0.394). The orthorhombic distortion induces a twinning of the (a and b) axis with an interchange of the short and long axis in different domains of the crystal (Frello, 2000). This could explain the decrease of T_c for that sample.

The enhancement in the superconducting properties are resulting from the uniform distribution of carriers in internal and external planes with the promotion of doping Au nanoparticles at copper sites in the CuO_2 planes depend upon the oxygen contents in the charge reservoir layer (CuO_2) and the oxygen contents lead to the influence on the crystalline phase of superconductor. The T_c , $T_{c R=0}$ and ΔT_c values found from the R-T plots show a combined effect of Pb and Au nanoparticles in the Bi-2223 phase, the transition width ΔT_c increased with the increasing of Au-nano addition concentrations except for the 0.6wt% sample which show less difference between T_c and ΔT_c . Such results are compatible with those obtained from XRD. However, for all the samples with Au-nano additions, the transition to T_0 is nearly one step transition, indicating the formation of nearly (Bi,Pb)-2223 single phase.

Table 2. Critical temperature T_c , $T_{c R=0}$, transition width ΔT_c , carrier concentration p , oxygen contents δ , and Volume Fractions of Both Low and High Tc phases for different nano-Au added concentration.

Nano-Au wt%	T_c (K)	T_0 (K)	ΔT_c (K)	δ	p
0.0	110	103	7	0.0437	0.132
0.2	114	101	13	0.0879	0.128
0.4	116	100	16	0.241	0.127
0.6	112	98	14	0.394	0.124
0.8	120	102	18	0.325	0.130
1.0	123	103	20	0.149	0.132

All samples were used as targets to prepare high-quality superconducting thin films by Pulsed Laser Deposition. The properties and structures of these films are mainly controlled by the concentration and the composition of the targets for ablation. X-ray diffraction pattern of the prepared films are shown in Figure 3. It can be noticed the presence of both high and low phases with the high phase being the dominant one. Also, all films are well crystallized having orthorhombic phase with *c*-axis oriented perpendicular to the film surface. An unknown phase having peaks 21.3° clearly appears in all samples. Also, for the Au nanoparticles added films a sharpness for some peaks such as H(0012) and H(0016) have been noticed. This may be attributed to the change in the oxygen content of the films. The slightly shifted peaks for Au in comparison to the value of the (Bi,Pb)-2223 when appearance of a new peak at a value of $2\theta = 11.28^\circ$. Furthermore, the unknown peaks may be attributed to the identified by an increase in the gradual annealing temperature for thin films at 400°C that remains constant for 0.5 hr may be resulted in the formation of Ca_2PbO_4 and Bi_2CuO_4 phases along with traces of CuO as secondary phase (Mua, Sundaresan, kman, & Dung, 2014). Then the annealing temperature continues rises until it reached 800°C and remains for 1.5 hr to complete with the oxidation process. The presence of a CuO phase beyond 800°C, that might be due to the decomposition of Bi_2CuO_4 with increasing intensity of the peaks for Ca_2PbO_4 , i.e. this indicates that the Bi-2212 phase decomposes into the Bi-2223 phase under periods of the annealing. These results show that it is difficult for a major Bi-2223 phase to form below 800°C, but it appears at temperatures equal or higher than 800°C or for longer annealing times, these results are in good agreement with those reported by Nono et al. (2015). Due to the annealing treatment of the films a crystalline order was established and an improvement of the films morphology, optimization of oxygen content and a change of the phase composition of the films have been obtained.

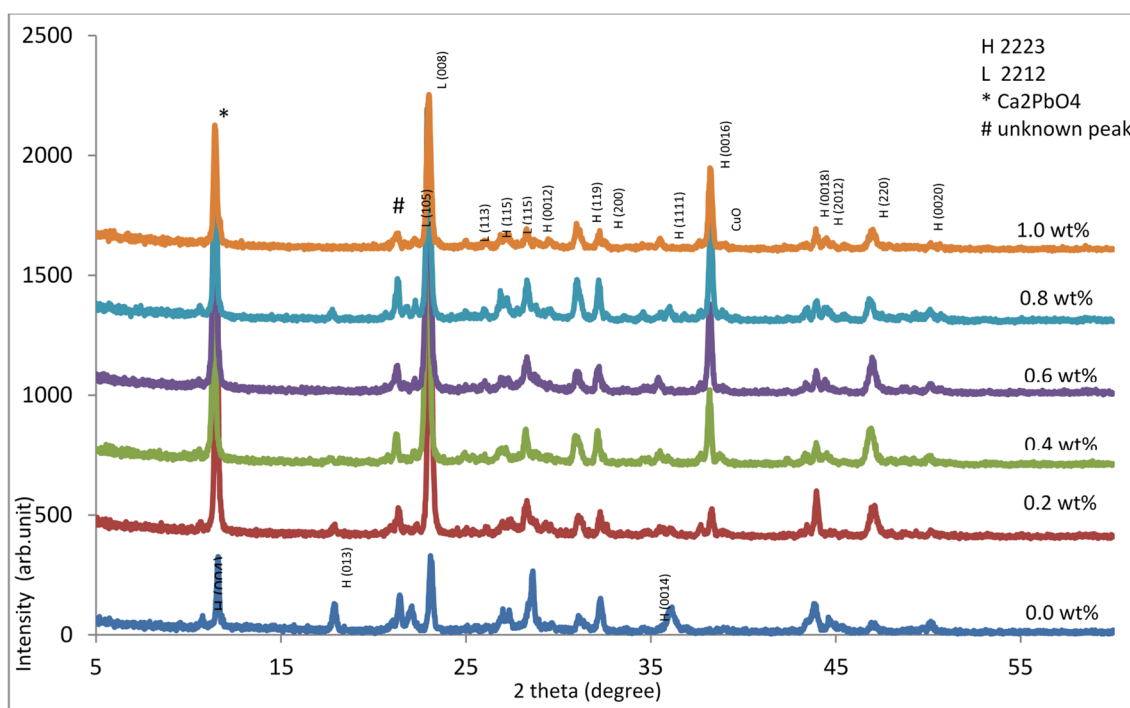


Figure 3. X-Ray diffraction patterns of Bi(Pb)-2223 thin films with different Au nanoparticles addition.

By analyzing the intensities of diffracted x-ray beams the crystal structures have been solved and may be used to measure the average crystal size of the sample. The lines in a thin film diffraction pattern are of finite breadth but if the particles are very small, the lines are broadened than usual. The broadening decreases with the increase in particle size. The particles size for Bi-2223 phase was calculated from x-ray diffraction patterns of strong reflections with intensity (%) by measuring the full width at half maximum (FWHM). The Debye Scherrer equation for calculating the particle size is given by (Nair et al., 2014):

$$D = \frac{\kappa\lambda}{\beta \cos \theta} \tag{3}$$

Where: K is the shape factor, it can assume values ranging from (0.89) which accounts for the shape of the particle. λ is the wavelength of copper $K\alpha = 1.5405 \text{ \AA}$. β is the full width at half maximum. θ is the measured angle. The particles size of the films is shown in the Table 3. Some particle sizes increase with the increasing of Au nanoparticles concentration, probably due to the decrease of the system melting point induced by the nanoparticles addition. It can be notice from the table that most of the average diameter is less than 100 nm.

Table 3. Grain size of thin films samples with different Au nanoparticles addition concentrations grown at 800°C on a Si (111) substrate

Nano-Au wt%	(D) Crystallite Size for Bi-2223 phase (nm)									
	Ca ₂ PbO ₄	(013)	(115)	(0012)	(119)	(1111)	(0016)	(0018)	(220)	D (av.) nm
0.0	69.89	57.08	84.05	44.19	54.8	172.1	-	28.25	31.71	67.76
0.2	73.26	118.62	43.91	40.29	54.8	-	42.21	38.7	19.03	53.85
0.4	85.63	-	62.26	46.66	46.28	-	42.28	38.7	19.71	49.36
0.6	62.24	-	53.94	52.12	38.38	-	38.48	39.71	22.46	43.91
0.8	74.46	57.1	59.57	29.15	52.1	-	42.55	36.73	23.22	46.86
1.0	73.66	-	48.58	38.59	50.18	-	44.19	38.06	24.68	45.42

The lattice relationship between the substrate and the thin film proved to be a strong tool to induce the film orientation. The lattice constant of thin films was calculated using (hkl) values of the strong peaks in the XRD patterns with the aid of Bragg's law. Increasing the addition of Au nanoparticles to $x=1.0$ wt% slightly enhanced the lattice parameters. The length may be expanded or contracted with the change of the electrons into antibonding orbital. Indeed, the behavior of the lattice constant may attribute to the displacement of Bi^{+1} ions inside the structure. The variations of lattice parameters indicate the intercalation of oxygen species. This change of a and c effect the volume of the unit cell and then causes variation of the density. The increase in volume is attributed to a larger number of Cu-O layers in the unit cell with the addition of Au nanoparticles. The lattice parameters, unit cell volumes, and the ratio c/a for the prepared films are listed in Table 4. The values of c/a for the films indicate the chalcopyrite structure for those samples.

It can be observe that the value of c -lattice parameters for the films not subjected to Au additions is about $c=36.929$ while for Au added films the values lies in a range between $c=37.0460$ to 37.098 . The variation in c -lattice can be attributed to the decrease in the fraction of oxygen in the Au added samples. Hence, oxygen annealing is necessary for the as-deposited films. The annealing allows uniform diffusion for Bi(Pb)-2223 materials on Si(111) substrate forming smoother films. Also, it may increase copper oxides for intergrowth structure consisting of Au/BPSCCO layers of the oxygen concentration during the annealing which imparts isotropy for thin films. In general, the average c -axes length value is found to increase with the increase of nano-Au content. The elongation of c/a axes is generally associated with the increase in the Cu-O bond length in the Cu-O₂ planes, which controls the dimensions in the basal planes.

Table 4. Lattice parameters and unit cell volumes of Bi(Pb)-2223 thin films for different nano-Au addition

Nano-Au wt%	$a \text{ \AA}$	$b \text{ \AA}$	$c \text{ \AA}$	Volume (V) (\AA^3)	$\frac{c}{a}$	ρ_M (g/cm^3)	Volume Fraction	
							HTC%	LTC%
0.0	5.390257	5.401936	36.92936	1075.3025	6.8511	1.581	59.85	40.15
0.2	5.541248	5.388601	37.04605	1106.1792	6.6855	1.537	51.89	48.11
0.4	5.544259	5.398784	37.07472	1109.73	6.6871	1.531	52.39	47.61
0.6	5.544007	5.377416	37.08191	1105.5018	6.6887	1.537	56.44	43.56
0.8	5.540641	5.371831	37.08824	1103.8716	6.6939	1.534	62.11	37.89
1.0	5.542017	5.398493	37.09838	1109.9293	6.6940	1.532	69.07	30.93

The SEM micrographs of the cross-sectional view for $Bi_{1.7}Pb_{0.3}Sr_2Ca_2Cu_3O_{10+\delta}$ and some Au nanoparticles added films are shown in Figures 4. The SEM shows that the microstructures are influenced by the Au addition when we have optimized a post-annealing treatment. SEM observations confirm that we obtain large grains lying parallel to the substrate. As shown by the arrows in the images. It can be noticed that the prevalence of small

homogeneous grains size for Au/Bi(Pb)-2223 on the film. Furthermore, the many grain boundaries and voids could be seen for the films on Si due to a large lattice mismatch. Relatively, smooth films with a surface roughness, a grain size of a range (50 - 500) nm and a low particulate density were obtained on Si substrate (Mua, Sundaresan, kman, & Dung, 2014). The difference in the grain size and the distribution of grains on the surface of the samples indicate the influence of replacing of Au^{+1} and Pb^{+2} together for Bi-2223 on the morphology of the samples. The image of 1.0 wt% nano-Au concentration shows large grains size with thin plate-like and needle-like structures. The grain structures were aligned to make more dense and conductive sample.

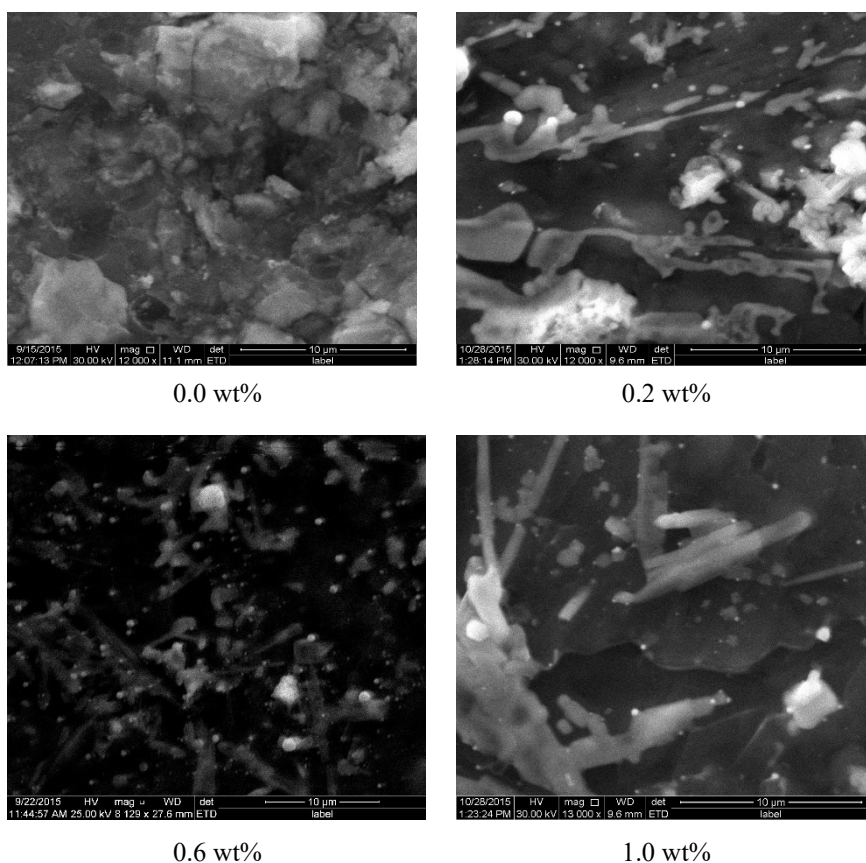


Figure 4. SEM Micrographs of Bi(Pb)-2223 phase for different Au nanoparticles added films

The resistivity versus temperature measurements of the films are shown in Figure 5. All samples have shown a metallic variation in the resistivity from room temperature down to onset of superconductivity. It can be observed that the electrical properties are modified, T_c value increased with the increasing of Au concentration to $x=1.0$ wt% except for $x=0.2$ wt% which show T_c less than 100K as listed in Table 5. However, the transition from normal to superconducting state is broad, suggesting a rather high disorder in the structure. This may be attributed to the oxygen concentration fluctuation in grains, which the critical temperature is very much dependent on. It is interesting to notice that the resulting inhomogeneity in oxygen concentration would lead to variations in the structural parameters, as observed in the XRD patterns which confirm this viewpoint.

Sharpness of transition is defined as the difference between $T_c(\text{onset})$ and $T_c(\text{zero})$. The T_c value of the films had increased to 110K as the addition concentration of Au nanoparticles increased to 1.0wt%, but the sharpness of the transition was the weakest. The initial increase in the sharpness of the superconducting transition indicates that the superconducting domains that are present in the film get coupled better and increasing the homogeneity of the films. This result is compatible to that obtained from the SEM images.

It can be noticed that ΔT value for all the films increases with the increasing of nano-Au addition, especially for the $x=1.0$ wt% sample which showed the highest value of the critical temperature, while the sample $x=0.2$ wt% showed the lowest values of ΔT and T_c . The thickness of the thin films could have an effect on the results of the

critical temperature, grains size and the films growth because if a crystal has its wide planar *c*- axis of the surface in contact with another surface it can reduce the surface energy with the potential for so adhere to the surface. The critical temperature T_c , $T_{c R=0}$ transition width ΔT_c and carrier concentration p of Bi(Pb)-2223 phase thin films for different Au nanoparticles addition are listed in Table 5.

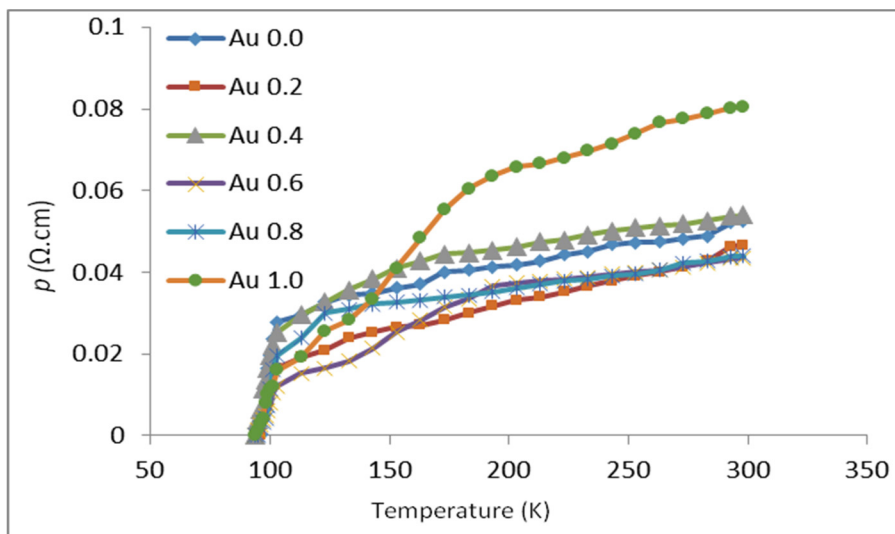


Figure 5. ρ -T plots of $\text{Bi}_{1.7}\text{Pb}_{0.3}\text{Sr}_2\text{Ca}_2\text{Cu}_3\text{O}_{10}$ thin films with different Au nanoparticles addition

Table 5. Critical temperature $T_c, T_{c R=0}$, transition width ΔT_c and carrier concentration p of $\text{Bi}_{1.7}\text{Pb}_{0.3}\text{Sr}_2\text{Ca}_2\text{Cu}_3\text{O}_{10+\delta}$ thin films with different Au nanoparticles addition

(Nano-Au) wt%	T_c (K)	T_0 (K)	ΔT (K)	p
0.0	100	98	2	0.123
0.2	98	96	2	0.121
0.4	101	97	4	0.122
0.6	103	97	6	0.122
0.8	105	96	8	0.121
1.0	110	97	13	0.122

To clarify that Au nanoparticles plays an important role in enhancement the Bi(Pb)-2223 phase of the thin films, also for checking the differences in the surface morphologies, the surface morphology for different films was carried out by using AFM measurement. The AFM surface images for all thin films are shown in Figure 6. The images reveals spherical shape and rod-like with average diameter 104.65 nm. Roughness average (RA) values and the root mean square deviation value (RMS) from the images are 2.3 nm and 2.66 nm respectively for the 0.0 wt% film. On the other hand, the average surface roughness is (0.348 - 6.44) nm for 0.2-1.0 wt% films respectively. The larger grains (e.g. rod-like) were superposed overlapping sites of Bi(Pb)-2223 thin films with nano-Au particles, even blends with each other in the layer-by-layer deposition process. Evidently, this overlapping occurred because of the low surface mobility at room temperature, wherever a stress existed between the Au crystal and the Bi(Pb)-2223 interface. This can be ascribed also to the increase of oxygen content in the film grains as consequence of the oxidation during the annealing with flow oxygen (O_2). Also, as indicated from XRD It seems that higher temperatures are necessary to activate particle diffusion. Because of this, the absolute value of the temperature rise during the annealing that led to the surface roughness and an increase in the average diameter as the Au concentration increased from 0.2 to 1.0 wt%. This result permits to conclusion of the size of grain is dependent on the annealing temperature, as shown in Table 6.

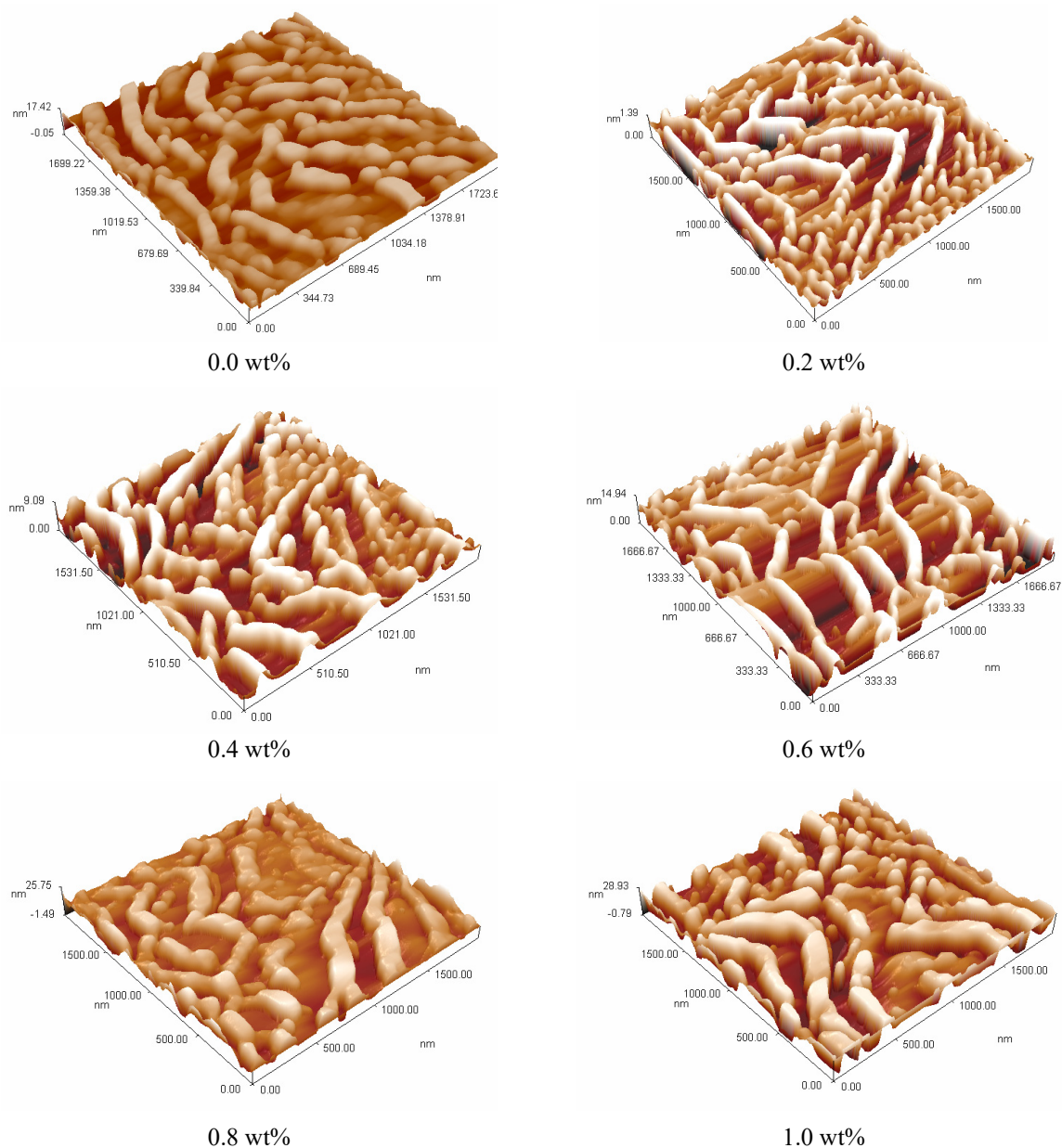


Figure 6. AFM surface image of Bi(Pb)-2223 thin films for different Au nanoparticles addition after annealing at 800°C on a Si substrate

Table 6. Average diameter, average surface roughness (RA) and root mean square (RMS) deviation of Bi(Pb)-2223 thin films for different Au nanoparticles addition after annealing at 800°C on a Si substrate

(nano-Au) wt%	Sa (Roughness Average) nm	Sq (Root Mean Square) nm	Avg. Diameter nm
0.0	2.3	2.66	104.65
0.2	0.348	0.401	80.30
0.4	2.27	2.62	93.57
0.6	3.58	4.27	99.30
0.8	3.69	4.29	98.67
1.0	6.44	7.46	99.23

4. Conclusions

This paper reports on the effects of Au nanoparticle on the superconducting properties of $\text{Bi}_{1.7}\text{Pb}_{0.3}\text{Sr}_2\text{Ca}_2\text{Cu}_3\text{O}_{10}$ thin films that have been prepared via Pulsed Laser Deposition (PLD) method. The addition of Au nanoparticles to the compound was investigated by introducing nanoparticles (0.0 - 1.0) wt. % within the structures of the superconductors. The XRD pattern shows that the addition of Au nanoparticle does not change the crystallographic structure of the samples and remain in an orthorhombic unit cell, the c-axis of the samples has slightly increased with increasing Au nanoparticles addition. The volume fraction as well as T_c have been increased. The highest volume fraction of the Bi(Pb)-2223 phase 77.24% and the best value for T_c of 110 K has been obtained from the sample with 1.0 wt.% as against 100 K for the non-added thin films. An important microstructural/structural characteristic found that increasing Au addition to 1.0 wt% increases the formation of randomly bigger platelet grains size on the surface (compact platelets), forms of a needle (or rod) and flowers.

References

- Maeda, H., Tanaka, Y., Fukutomi, M., & Asano, T. (1988). A new high- T_c oxide superconductor without a rare earth element. *Jpn. J. Appl. Phys.*, 27, L209–L210.
- Verma, I., Kumar, R., Ganesan, V., Banerjee, A., & Das, B. (2012). Synthesis and Magnetic Properties of $(\text{Bi,Pb})_2\text{Sr}_2\text{Ca}_2\text{Cu}_3\text{O}_{10+\delta}$ Superconductor. *J. Supercond. Nov. Magn.*, 25, 785–789. <http://dx.doi.org/10.1007/s10948-011-1339-6>.
- Díaz-Valdés, E., Pacheco-Malagón, G., Contreras-Puente, G., Mejía-García, C., Andrade-Garay, G., Ortíz-López, J., ... Falcony, C. (1993). Effect of lead content on nonstoichiometric $\text{Bi}_{2-x}\text{Pb}_y\text{Sr}_2\text{Ca}_2\text{Cu}_3\text{O}_\delta$ ceramic superconductors. *Materials Chemistry and Physics*, 36(1-2), 64-67. [http://dx.doi.org/10.1016/0254-0584\(93\)90008-A](http://dx.doi.org/10.1016/0254-0584(93)90008-A).
- Mua, N. T., Sundaresan, A., kman, N., & Dung, D. D. (2014). Influence of preparation conditions on superconducting properties of Bi-2223 thin films. *Bull. Mater. Sci.*, 37(1), 19–25.
- Jannah, A. N., Halim, S. A., & Abdullah, H. (2009). Superconducting Properties of BSCCO Thin Films by Pulsed Laser Deposition. *European Journal of Scientific Research*, 29(4), 438-446.
- Abbas, M. M., Oboudi, S. F., & Raouf, N. Q. (2015). Investigating the Preparation Conditions on Superconducting Properties of $\text{Bi}_{2-x}\text{Li}_x\text{Pb}_{0.3}\text{Sr}_2\text{Ca}_2\text{Cu}_3\text{O}_{10+\delta}$, *Materials Sciences and Applications*, 6, 310-321. <http://dx.doi.org/10.4236/msa.2015.64036>.
- Jeremie, A., Alami-Yadri, K., Grivel, J. C., & Flükiger, R. (1993). Bi,Pb(2212) and Bi(2223) formation in the Bi-Pb-Sr-Ca-Cu-O system. *Superconductor Science and Technology*, 6(10), 730-735.
- Sozeri, H., Ghazanfari, N., Ozkan, H., & Kilic, A. (2007). Enhancement in the high- T_c phase of BSCCO superconductors by Nb addition. *Supercond. Sci. Technol.*, 20, 522-528.
- Jabbar, A., Qasim, I., Mumtaz, M., & Nadeem, K. (2015). Synthesis and superconductivity of $(\text{Ag})_x/\text{CuTi-1223}$ composites, *Progress in Natural Science: Materials International*, 25(3), 204-208. <http://dx.doi.org/10.1016/j.pnsc.2015.06.001>
- Zelati, A., Amirabadizadeh, A., Kompany, A., & Salamati, H. (2014). Effect of Eu_2O_3 Nanoparticles Addition on Structural and Superconducting Properties of BSCCO. *Journal of Superconductivity and Novel Magnetism*, 27, 1369-1379. <http://dx.doi.org/10.1007/s10948-013-2475-y>
- Hafiz, M., & Abd-Shukur, R. (2015). Effect of Nanosized NiF_2 Addition on the Transport Critical Current Density of Ag-Sheathed $(\text{Bi}_{1.6}\text{Pb}_{0.4})\text{Sr}_2\text{Ca}_2\text{Cu}_3\text{O}_{10}$ Superconductor Tapes. *Advances in Materials Science and Engineering*, 1-5. <http://dx.doi.org/10.1155/2015/146476>
- Farbod, M., & Batvandi, M. R. (2011). Doping effect of Ag nanoparticles on critical current of $\text{YBa}_2\text{Cu}_3\text{O}_7$ bulk superconductor. *Physica C*, 471, 112-117.
- Miura, M., Mukaida, M., Matsumoto, K., Yoshida, Y., Ichinose, A., Horii, S., Kita, R., Saito, A., Kaneko, K., Yamada, K., & Mori, N. (2006). Surface resistance of RE123 films with artificial pinning centers. *Physica C*, 845–848, 828-832.
- Mumtaz, M., Khan, N. A., & Khan, E. U. (2010). Growth of $\text{Cu}_{0.5}\text{Tl}_{0.5}\text{Ba}_2\text{Ca}_3\text{Cu}_{4-y}\text{Zn}_y\text{O}_{12-\delta}$ superconductor with optimum carriers. *Physica C*, 470, 428-434.
- Nadeem, K., Naeem, F., Mumtaz, M., Naeem, S., Jabbar, A., Qasim, I., & Khan, N. A. (2014). Synthesis and characterization of core-shell Ni/NiO nanoparticles/CuTi-1223 superconductor composites. *Ceram. Int.*, 40, 13819–13825.

- Suazlinaa, M. A., Yusainee, S. Y. S., Azhan, H., Abd-Shukor, R., & Mustaqim, R. M. (2014). The Effects of Nanoparticle Addition in Bi-2212 Superconductors. *Jurnal Teknologi (Sciences & Engineering)*, 69(2), 49–52.
- Ishii, A., & Hatano, T. (2000). Preparation of high quality $\text{Bi}_2\text{Sr}_2\text{CaCu}_2\text{O}_{8+\delta}$ thin films on a MgO substrate by pulsed laser ablation and post-annealing recrystallization of films accompanying in-plane rotation of a and b axes. *Physica C*, 340, 173.
- Suvasis, S. (2011). Studies on Superconductor/Nano Composite of BSCCO/BiFeO₃, M.Sc. Thesis, Department of Physics, National Institute of Technology Rourkela, India.
- Ki Young, S., & Soo Lee, M. (2006). The effect of a large amount of Ag introduced into the $\text{Bi}_{1.84}\text{Pb}_{0.34}\text{Sr}_{1.91}\text{Ca}_{2.03}\text{Cu}_{3.06}\text{O}_{10+\delta}$ (110 K phase) high- T_c superconductor. *IOP Superconductor Science and Technology*, 19(12), 1253-1258.
- Hermiz, G. Y., Abbass, M. M., & Gilioli, E. (2009). Superconductivity of $(\text{Bi}_{0.7}\text{Pb}_{0.3})_2\text{Bi}_x\text{Sr}_2\text{Ca}_2\text{Cu}_3\text{O}$ ($0 < x < 0.5$). *Atti Della, Fondazione Giorgio Ronchi, Anno Lxiv*, 1-8.
- Ramadan, A. A., Abdel-Hady, S., Abdel-Ghany, S., & Soltan, S. E. (2000). Flash Evaporation as an Attempt for Preparation of YBCO Superconductor Thin Films. *Egypt. J. Sol.*, 23(1), 59-69.
- Zargar Shoushtari, M., & Mousavi Ghahfarokhi, S. E. (2011). A Study of the Magnetic Properties of $\text{Bi}_{1.64-x}\text{Pb}_{0.36}\text{Cd}_x\text{Sr}_2\text{Ca}_2\text{Cu}_3\text{O}_y$ Superconductor. *Journal of Superconductivity and Novel Magnetism*, 24, 1505-1511. <http://dx.doi.org/10.1007/s10948-010-0899-1>
- Mawassi, R., Marhaba, S., Roumié, M., Awad, R., Kork, M., & I. Hassan, I. (2014). Improvement of Superconducting Parameters of $\text{Bi}_{1.8}\text{Pb}_{0.4}\text{Sr}_2\text{Ca}_2\text{Cu}_3\text{O}_{10+\delta}$ Added with Nano-Ag. *Journal of Superconductivity and Novel Magnetism*, 27(5), 1131–1142.
- Ahmed, A. R. (2015). Study of the Electrical and Structural/Micro structural Properties of $\text{Bi}_{2-x}\text{Bi}_x\text{Ba}_{2-y}\text{Sr}_y\text{Ca}_2\text{Cu}_3\text{O}_{10+\delta}$ System. *IISTE Advances in Physics Theories and Applications*, 39, 33-42.
- Soo Lee, M. (2003). Microstructure and Superconducting Properties of (Bi,Pb)-Sr-Ca-Cu-O-(Ag, Au, Mg) Composites. *Journal of the Korean Ceramic Society*, 40(5), 447-454.
- Ozturk, O., T. Küçükömeröğlu T., & Terzioglu, C. (2007). Calculation of the diffusion coefficient of Au in Bi-2223 superconductors. *IOP Publishing Ltd., Journal of Physics: Condensed Matter*, 19(34), 346205.
- Jabbar, A., Qasim, I., Khan, K. M., Ali, Z., Nadeem, K., & Mumtaz, M. (2015). Synthesis and superconducting properties of $(\text{Au})_x/\text{CuTi-1223}$ composites. *Elsevier B.V., Journal of Alloys and Compounds*, 618, 110–114.
- Frello, T. (2000). Structural and Superconducting Properties of High- T_c Superconductors. *Riso National Laboratory, 1086(EN)*, Roskilde, Denmark.
- Nono, D., Imaduddin, A., Raju, K., & Dang-Hyok, Y. (2015). Synthesis and Characterization of $\text{Bi}_{1.6}\text{Pb}_{0.4}\text{Sr}_2\text{Ca}_2\text{Cu}_3\text{O}_7$ Superconducting Oxide by High-Energy Milling. *J Supercond Nov Magn*, 28(8), 2259–2266.
- Nair, A. S., Vinila, V. S., Issac, S., Jacob, R., Mony, A., Nair, H. G., Rajan, S., Satheesh, D. J., & Isac, J. (2014). Studies on Nano Crystalline Ceramic Superconductor $\text{LaZrYBaCa}_2\text{Cu}_3\text{O}_{11}$ at Three Different Temperatures. *Journal of Crystallization Process and Technology*, 4, 126-133.

Copyrights

Copyright for this article is retained by the author(s), with first publication rights granted to the journal.

This is an open-access article distributed under the terms and conditions of the Creative Commons Attribution license (<http://creativecommons.org/licenses/by/4.0/>).